

Form Approved
OMB No. 0704-0188

1. REPORT DATE (DD-MM-YYYY)

2. REPORT TYPE

3. DATES COVERED (From - To)

5a. CONTRACT NUMBER

5b. GRANT NUMBER

5c. PROGRAM ELEMENT NUMBER	
----------------------------	--

6. AUTHOR(S)

5d. PROJECT NUMBER	
--------------------	--

5e. TASK NUMBER

5f. WORK UNIT NUMBER

7. PERFORMING ORGANIZATION NAME(S) AND ADDRESS(ES)

8. PERFORMING ORGANIZATION REPORT

9. SPONSORING / MONITORING AGENCY NAME(S) AND ADDRESS(ES)

10. SPONSOR/MONITOR'S ACRONYM(S)

Air Force Research Laboratory (AFMC)
AFRL/PRS
5 Pollux Drive
Edwards AFB CA 93524-7048

11. SPONSOR/MONITOR'S
NUMBER(S)

12. DISTRIBUTION / AVAILABILITY STATEMENT

Approved for public release; distribution unlimited.

13. SUPPLEMENTARY NOTES

14. ABSTRACT

20030116 058

15. SUBJECT TERMS

16. SECURITY CLASSIFICATION OF:

17. LIMITATION OF ABSTRACT

18. NUMBER
OF PAGES

19a. NAME OF RESPONSIBLE PERSON

a. REPORT

b. ABSTRACT

c. THIS PAGE

Unclassified

Unclassified

Unclassified

19b. TELEPHONE NUMBER

(include area code)
(661) 275-5015

MEMORANDUM FOR PR (Contractor/In-House Publication)

FROM: PROI (TI) (STINFO)

30 Jun 2000

SUBJECT: Authorization for Release of Technical Information, Control Number: **AFRL-PR-ED-TP-2000-145**
B. Chehroudi (ERC); R. Cohn, D. Talley (AFRL/PRSA); A. Badakhshan (University of Northern Iowa),
"Raman Scattering Measurement in the Initial Region of Sub- and Supercritical Jets"

36th AIAA/ASME/SAE/ASEE Joint Propulsion Conference and Exhibit
(Huntsville, AL, 17-19 Jul 00)

(Statement A)

(Submission Deadline: 13 Jul 00)

1. This request has been reviewed by the Foreign Disclosure Office for: a.) appropriateness of distribution statement, b.) military/national critical technology, c.) export controls or distribution restrictions, d.) appropriateness for release to a foreign nation, and e.) technical sensitivity and/or economic sensitivity.

Comments: _____

Signature _____

Date _____

2. This request has been reviewed by the Public Affairs Office for: a.) appropriateness for public release and/or b) possible higher headquarters review.

Comments: _____

Signature _____

Date _____

3. This request has been reviewed by the STINFO for: a.) changes if approved as amended, b.) appropriateness of distribution statement, c.) military/national critical technology, d.) economic sensitivity, e.) parallel review completed if required, and f.) format and completion of meeting clearance form if required

Comments: _____

Signature _____

Date _____

4. This request has been reviewed by PR for: a.) technical accuracy, b.) appropriateness for audience, c.) appropriateness of distribution statement, d.) technical sensitivity and economic sensitivity, e.) military/national critical technology, and f.) data rights and patentability

Comments: _____

APPROVED/APPROVED AS AMENDED/DISAPPROVED

LESLIE S. PERKINS, Ph.D
Staff Scientist
Propulsion Directorate

(Date)

AIAA 2000-3392

Raman Scattering Measurement in the Initial Region of Sub- and Supercritical Jets

B. Chehroudi^{}, R. Cohn[#], D. Talley[#], and A. Badakhshan[†]*

^{*} Engineering Research Corporation Inc
10 E. Saturn Boulevard
Edwards AFB, CA 93524-7680

[#] Air Force Research Laboratory
Propulsion Directorate
10 E. Saturn
Edwards AFB

[†] Department
University of
1620 Birch St.
Cedar Falls, IA

*Revisions to English & Grammar
in progress; no changes will be
made in technical content.*

**36th AIAA/ASME/SAE/ASEE
Joint Propulsion Conference and Exhibit
17-19 July, 2000
Huntsville, Alabama**

Raman Scattering Measurement in the Initial Region of Sub- and Supercritical Jets

B. Chehrودي*, R. Cohn[#], D. Talley[#], and A. Badakhshan⁺

*Engineering Research Corporation Inc.
10 E. Saturn Boulevard
Edwards AFB, CA 93524-7680

[#]Air Force Research laboratory
10 E. Saturn Boulevard
Edwards AFB, CA 93524-7680

⁺University of Northern Iowa
1620 Birch St.
Cedar Falls, IA 50613

Abstract

A high-pressure chamber is used to investigate and further enhance our knowledge and physical understanding on effects of thermodynamical subcritical-to-supercritical transition of ambient condition on cryogenic liquid injection using two-dimensional Raman scattering. Pure liquid N_2 is injected into N_2 . The injector is a 508 micron diameter straight hole having a long length-to-diameter ratio of 100. The optical setup uses a pulsed Nd:Yag laser frequency-doubled to 532 nm. Difficulties arise with optical breakdown of the N_2 molecules in drops and ligaments by local focusing of the laser beam dominating the Raman signal particularly at sub- and near-critical regions. The severity of this problem is reduced by stretching the laser pulse width using a double-loop design with mirrors and beam splitters. Careful and painstaking alignment is needed to take advantage of this pulse-stretcher design. Two-dimensional images are taken near the injector and results interpreted in terms of density plots. At subcritical ambient conditions a small number of images are needed for averaging and strong Raman signal is obtained. Substantial reduction of this signal is observed at supercritical condition due to jet radial growth and mixing. Radial intensity-surplus profiles are broadened by the interaction of the laser and the jet interface. The corrected profiles show a tendency towards the similarity profile seen for the gaseous turbulent jets near and above the critical point. Initial growth rate of the jet as judged by the Raman signature shows tendency towards gaseous turbulent jet when chamber pressure is raised from near the critical value and beyond. However, the difference remains quite distinct being nearly half the growth rate reported for gaseous jets. The initial growth rate is in reasonably-good agreement with our earlier measurements using shadowgraphy if twice the FWHM of the normalized intensity plots are used. Results are compared with gaseous jets and conclusions are drawn regarding effects of supercritical condition on the jet structure.

Introduction

It has been recognized that there were advantages in operating most power and thrust producing engines at higher combustion chamber pressures and temperatures

for enhanced efficiency and/or output thrust levels. In this paper, however, the main interest is on the cryogenic liquid-propulsion rockets. Progress in material science and technological achievements in designing vessels to withstand high pressure and temperature conditions bring us close to harness the theoretical gains in high pressure and temperature engine operation. However, there are some new issues that arise as a result of the elevated chamber conditions which must be understood for better engine design and performance predictability. One such issue is the realization that in cryogenic rockets, particularly under full throttle or take-off conditions, liquid propellants may find ~~be~~ injected into a thermodynamically supercritical condition. Our understanding of the injection under these conditions has been limited until recently when progress was made in both experimental and theoretical/computational areas, see, for example, Mayer *et al.* [1, 2], Chen and Sui [3], Woodward and Talley [4], Harstad and Bellan [5], Delplanque and Sirignano [6], Oefelein and Yang [7], and Chehrودي *et al.* [8, 9].

In most experimental works, initial attempts were to visualize the drop/jet formation and evolution using high speed photography techniques. Valuable information was gathered and analyzed using such methods and reported in the aforementioned publications. In an attempt to acquire a more detailed and quantitative information from fluid jets injected into supercritical condition, several laser diagnostics were evaluated and one of the most suitable candidate was identified to be the spontaneous Raman scattering, see Anderson *et al.* [10]. Raman scattering was used by Woodward and Talley [4], Decker *et al.* [11], and Oschwald and Schik [12], Oschwald *et al.* [13] to investigate the structure of the nitrogen fluid jet under supercritical condition. One of the fundamental difficulties in extracting true density information from the Raman effect was the uncertainty in the functional dependence of the Raman scattering cross section on temperature under these conditions. Raman cross section in liquids is larger (by 1.73 for LN_2 with $n=1.2$) than the gaseous phase by a correction factor that depends on the refractive index (n). Not being strictly a liquid, an estimate of 10% was given by Decker *et al.* [11] under supercritical condition for N_2 at 6 MPa. The other practical problem, enhanced by the lens effect of the liquid-like jet, is the onset of stimulated Raman scattering

*all units (if no hyphen bwn it and #) has a space bwn it and 1
The#

sub-script?

stet

g. I can w

g. 1 can withstand
137 atm (2000 psi)

—iv—

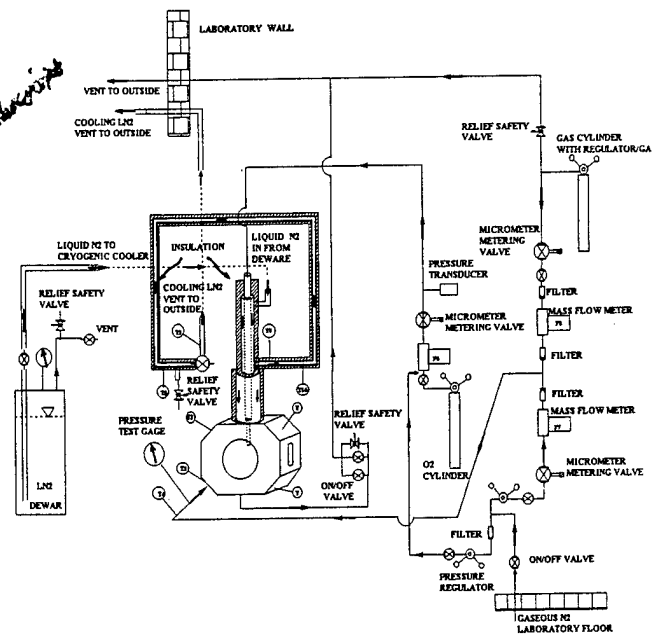


Figure 1. Schematic diagram of experimental setup for sub- to supercritical jet injection

Optical Setup

An Nd:Yag pulsed laser, model Powerlite 8010 by Continuum Corp. , was used at 532 nm and 800 mJ/pulse as the source to induce Raman effect. The repetition rate for this laser is 10 Hz with pulse width of 10 ns. To reduce possibility of the plasma formation a passive pulse stretcher was designed as shown in Fig. 2. The laser beam passes through three adjustable pinholes (PH1, PH2, and PH3) positioned at sufficient distances to allow periodic inspection of the incident beam alignment. Because the laser cavity was located on a separate optical table, this arrangement was found to be a very effective method for realignment. Also, this was used to direct a He-Ne alignment laser beam collinear with the Nd:Yag for initial phase of the alignment procedure. Wavelengths

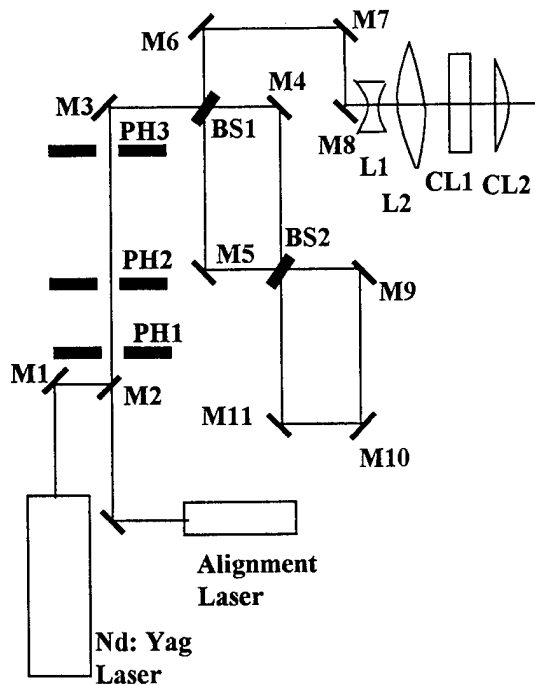


Figure 2. Schematic diagram of the laser beam/sheet path showing the delay loops and the alignment laser. BS (beam splitter), PH (pinhole), M (mirror), L (spherical lens), and CL (cylindrical lens).

not being the same, this initial alignment is near the final one which can ultimately be achieved when the Nd:Yag laser is used. This was found to be a safer and more efficient approach in usage of the Nd:Yag laser lifetime. In Fig. 2, the laser beam faces the first beam splitter at BS1 and about 35% of its intensity is split towards the M6 mirror. The remaining goes through the first loop (BS1-M4-BS2-M5-BS1) in about 8 ns of time. Note that only about 35% of this remaining energy is reflected by the mirror M5, the rest goes through the loop (BS2-M11-M10-M9-BS2) in another 8 ns time. Therefore, the original pulse is extended in time into three major pulses each being 10 ns in duration but delayed in time by 8 ns and 16 ns. The final pulse duration is about 36 ns. Precision laser mirrors with damage threshold of 10 J/cm² (10 ns pulse) and VIS coating from Edmond Scientific were used. The laser beam is shaped by passing through a Galilean beam expander (L1 & L2) before forming a thin sheet via two cylindrical lenses CL1 and CL2, see Fig. 2. The entire assembly, consisting of mirror M8 and all the lenses, are on a separate optical bench which can be traversed as a unit vertically (into the plane of Fig. 2) as well as in one horizontal direction. This gives sufficient flexibility to adjust and fix both the thickness of the sheet and its vertical and horizontal locations. The vertical and horizontal traverse directions provide axial and radial traverse capabilities, respectively.

The scattered Raman signal at 607 nm was detected by a nitrogen-cooled 256x256 CCD from Princeton Instrument equipped with a set of three filters. A high-pass OG570 filter was used to reduce the light at 532 nm by less than 10^{-5} and at 607 nm by not more than 0.9. A holographic supernotch filter blocked the light at 532 nm better than 10^{-4} while less than 0.8 at 607 nm. Finally, a narrow bandpass interference filter at 610 nm reduced the scattered light at 532 nm to better than 10^{-4} while attenuating by about 0.5 at 607 nm. Therefore, an optical density of better than 13 was achieved at 532 nm laser wavelength with the Raman signal transmittance of 0.36. This arrangement was found to be adequate to ensure removal of stray light while passing sufficient Raman for detection at 607 nm. The lens package consisted of a Nikon PK-12/14 extension ring connected to one end of a Noct-Nikkor 58 mm F/# (1.2 to 16) zoom lens with a NIK-2734 close-up lens located in its front.

A Summary of Previous Results

In the past two years, results from injections of several fluids into an ambient under both sub- and supercritical conditions at sufficiently high Reynolds numbers to be fully turbulent have been reported in the same test facility used here, see *Chehrودي et al.* [8,9]. A variety of ambient fluids was used into which pure N₂, He, and O₂ fluids were injected. The effects of chamber pressure (density) ranging from the thermodynamic subcritical to supercritical values at a supercritical chamber temperature (based on critical condition, P_c, T_c, of the injectant) were observed by acquisition of shadow images from the injector exit region using a CCD camera illuminated by short-duration light pulses. At sufficiently low subcritical chamber pressures, the disturbances on the jet interface amplified and eventually broke up downstream into irregularly-shaped small entities. Increasing the chamber pressure caused the formation of many small ligaments and droplets at the interface of the jet only within a narrow regime below the thermodynamic critical pressure of the injected pure fluid, resembling a second wind-induced liquid jet breakup. At even higher chamber pressures, near but below the critical pressure of the injectant, the expected transition into a full atomization regime to produce a liquid spray was inhibited due to sufficient reduction of both the surface tension and the heat of vaporization. The jet appearance changed abruptly at this pressure and resembled a turbulent gas injection for all higher chamber pressures. The jet initial growth rate was plotted together with available data on liquid fuel injection in diesel engine environments, and turbulent incompressible, supersonic, and variable-density jets and mixing layers. The resulting plot is unique on its own right covering four orders of magnitude in density ratio, see Fig. 3. At near- and super-critical pressures, these measurements agreed well with the theoretical growth rate equations proposed by *Brown* [15]/*Papamoschou and Roshko* [16] and *Dimotakis* [17] for incompressible but variable-density turbulent mixing layers. This constitutes the first quantitative evidence in support of

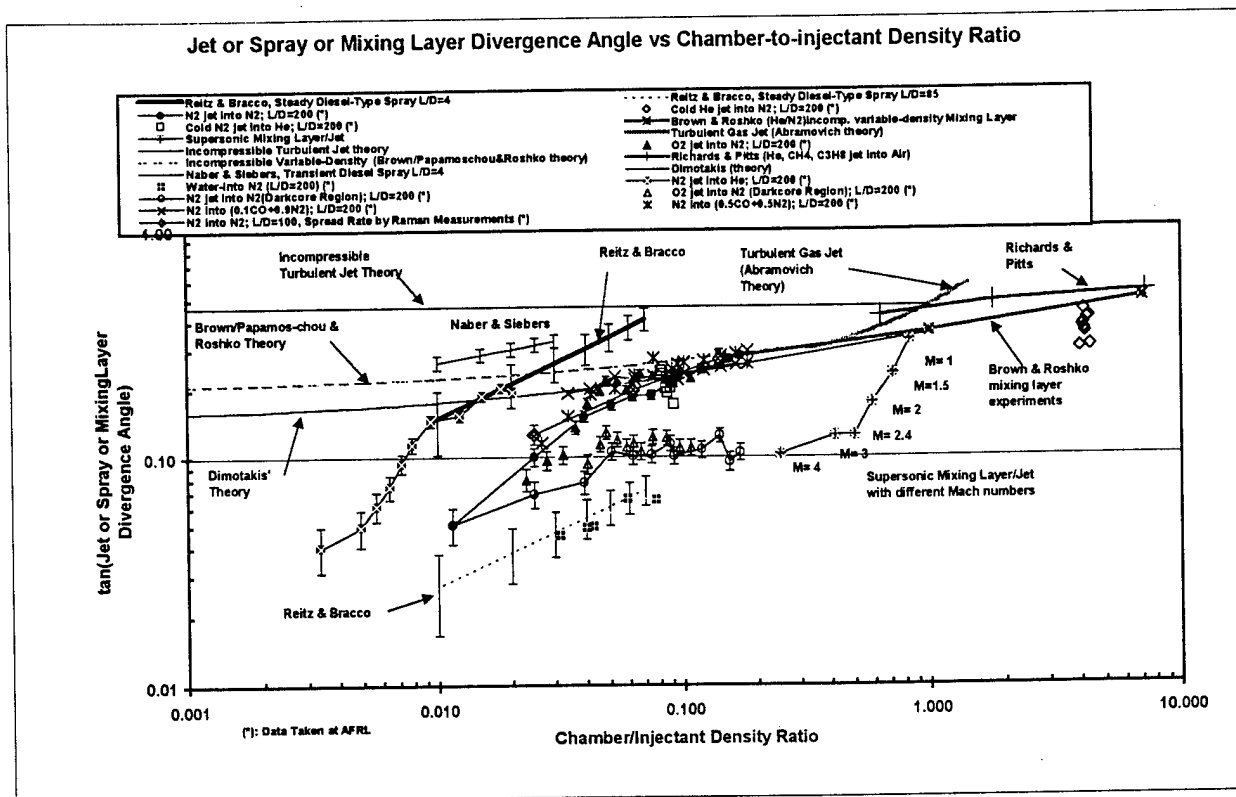


Figure 3. Initial growth rate of fluid jets as a function of the chamber-to-injectant density ratio for variety of cases.

the past qualitative observations that the jet appeared to evolve into a gas-like behavior. The geometry of the jet interface had also been examined for the first time by fractal analysis. The results clearly indicated a transition from a Euclidean to a fractal interface, with a fractal dimension close to values measured for gaseous turbulent jets. This provided an additional quantitative evidence for the hypothesis that the jet evolved into a gas-like behavior. Finally, an equation was proposed based on a physical model proposing that at the point of transition from liquid-like to gas-like appearances and the growth rates, the characteristic time of the vaporization is of the same order as the interfacial "bulge" formation/separation time. The model equation agreed well with the experimental growth rate data.

Experimental Results and Discussion

The first task prior to any image acquisition from the jets was to verify basic operation of the entire system. For this, it was decided to measure the Raman intensity from a pure gaseous nitrogen inside the high-pressure chamber at different chamber pressures. The ratios of the measured Raman intensities (corrected for the dark count) should be proportional to the density ratios calculated through an equation of state or thermodynamic tables. Figure 4 shows results from such a test.

In each column of this figure, gray scale (or false color, if seen in color) representation of the scattered Raman from the laser sheet is shown along with its 5-row-averaged intensity profile. The averaging is done within the two thick horizontal lines (covering 5 rows of pixels) shown in images. The lower edge of the laser sheet is clearly seen in each image and is where dark black zone meets the brighter color code. After removal of the dark-count from images, the measured intensity ratios are compared with those calculated using the ideal gas law for nitrogen. The agreement was quite satisfactory to within 2 percent.

When no LN2 was injected, the image acquisition procedure for each set consisted of an initial dark count image followed by images at three different chamber pressures (6.9, 2.82, and 1.46 MPa) similar to Fig. 4. This information was needed to remove dark count level and establish reference intensity levels at the aforementioned chamber pressures. They also served as a check for proper operation of the entire system setup. The Raman image acquisition from the LN2 jets at this same chamber pressures started subsequently.

Typical averaged (40 frames) raw images of the LN2 jet at subcritical and supercritical chamber conditions along with images characterizing the sheet profile at the measurement location are shown in Fig. 5. The actual measured intensity values were divided by 2 to accommodate the plots within the fixed Y-axis scale of

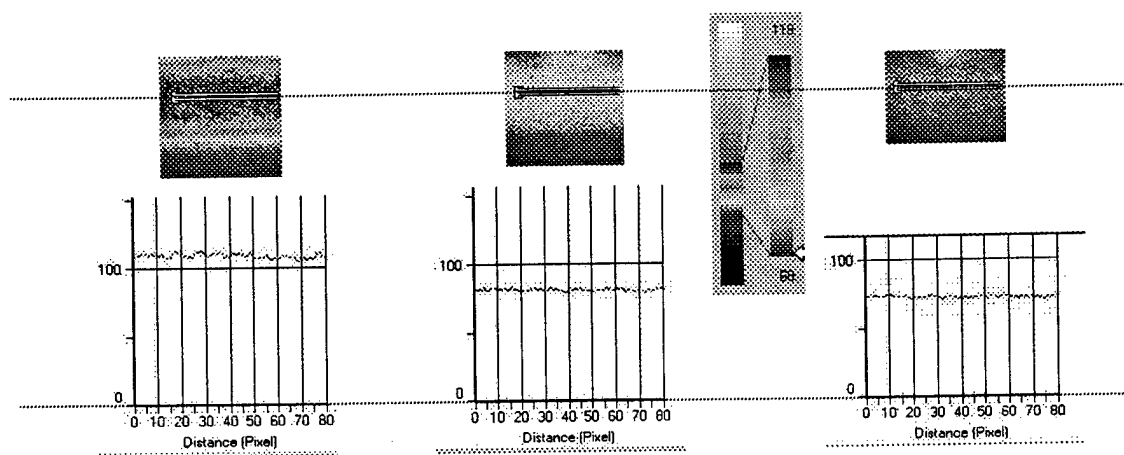
6.90 MPa (1000 psig)**2.82 MPa (400 psig)****1.46MPa (200psig)**

Figure 4. Raman intensity measured by passing the laser sheet into the chamber filled with N₂ at three different pressures.

the software. However, the conclusions reached from these plots are unchanged by such a scaling. Note that the Raman intensity profile for the subcritical case is higher in the center of the jet in magnitude and appears narrower in shape. With LN₂ injection, it was observed that the measured intensity well outside the jet area (representing the chamber density) was higher than when injection was turned off. This is due to the interaction of the laser and the jet, being particularly severe for the subcritical case where a clear sharp interface can be defined. This

interface caused reflection of a fraction of the laser contributing to higher measured Raman intensity values and noise levels. As an example, on the 40-framed-averaged images, when jet flow was off, the pixel-averaged measured Raman signals within a fixed rectangular region where laser entered the chamber were 101.4 and 70.6 units for the 6.9 MPa and 1.46 MPa cases, respectively; whereas the corresponding values for when the LN₂ jet was flowing were 116.4 and 98.0 units. Therefore, this defined a methodology for a first degree

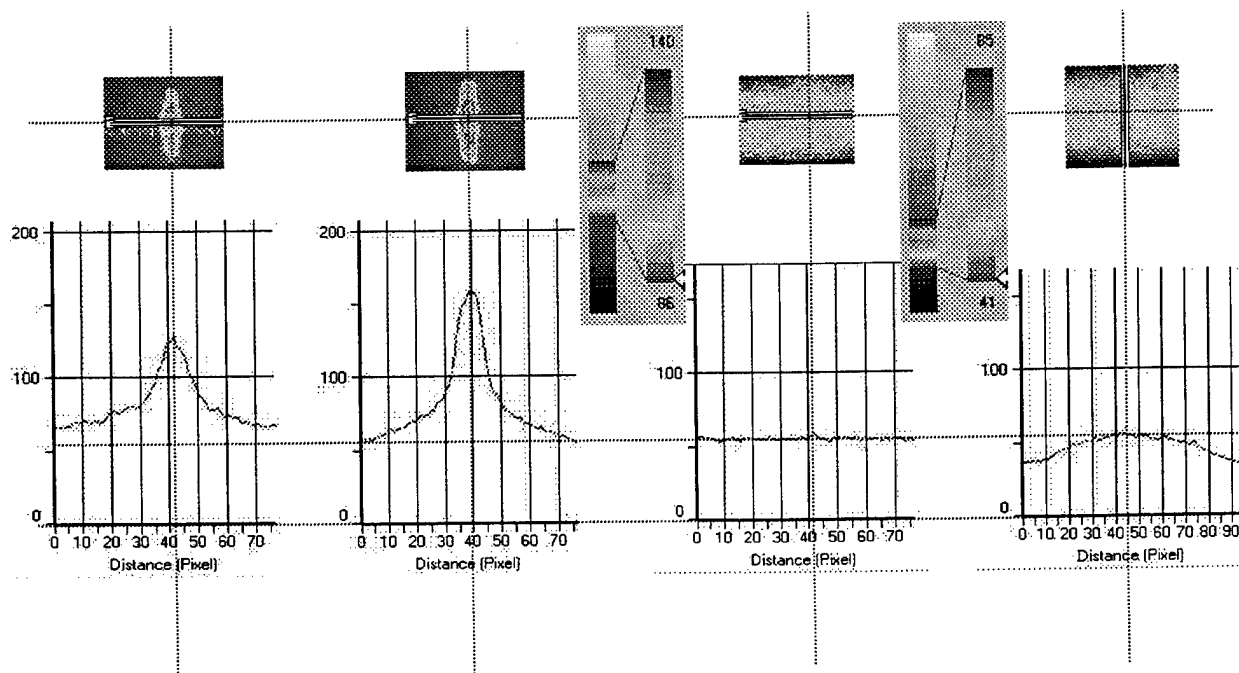
**Supercritical
6.9 MPa (1000 psig)****Subcritical
1.46 MPa (200 psig)****Laser Sheet Profile
6.9 MPa (1000 psig)**

Figure 5. typical 40-frame-averaged false-color images of the jet at sub- and supercritical chamber conditions. The laser sheet profile is also shown to be reasonably fat within the measurement region. Measured intensities are shown in each case.

correction to the raw data as follows. For each set of data at a given condition, Raman images were collected with no injection followed by the Raman images from the jets as described earlier. Using the example above, all pixel values for the 6.9MPa images were then reduced by $(116.4 - 101.4 = 15)$ and those for the 1.46 MPa by $(98.0 - 70.6 = 27.4)$. It is seen that this laser/jet interactional

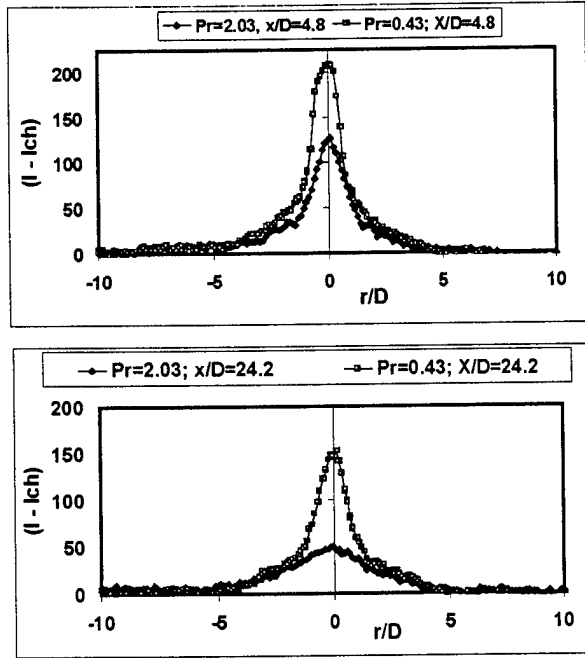


Figure 6. 40-frame-averaged Raman relative intensity radial profiles at two different distances from the injector and at sub- and supercritical chamber conditions.

contribution to the measured raw intensity is almost twice as much for the subcritical case indicating difficulty in complete removal of this side effect.

The test conditions for the Raman imaging were selected to correspond and complement our previously-reported shadowgraphy studies. Figure 6 Shows typical radial profiles of the 40-frame-averaged Raman intensities as measured with reference to the far field chamber intensity values at two distances from the injector exit plan and at sub- and supercritical chamber pressures. The laser sheet propagation direction is from right to left in this figure. Limitation for the number of frames were set by the combination of the acquisition/processing system and the practical operating time of the facility. However, it was found to be reasonably adequate. It is seen that the centerline intensity surplus $(I - I_{ch})$ declines away from the injector as well as when chamber pressure is raised to a supercritical value. Hence, reasonable trends are observed. One point of concern, however, is the existence of an unusual wide tail in these profiles particularly for the subcritical case. This issue will be discussed later. Figure 7 shows similarity-type plot of the intensity surplus at different axial distances and at sub- and supercritical conditions along with a proposed model for

turbulent jets. Note that according to *Wyganski and*

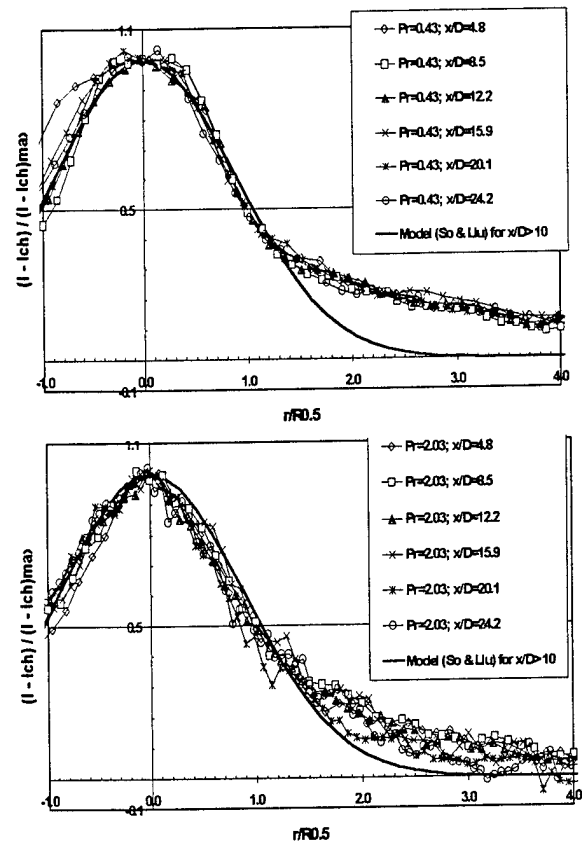


Figure 7. Similarity-type plot for the measured Raman intensity surplus $(I - I_{ch})$ at sub- (above) and supercritical (below) chamber conditions. $R0.5$ is the radius at which $(I - I_{ch})$ drops to half of its maximum.

Fiedler [18] fully self-preservation turbulent jet is observed for the velocity field at x/D of greater than 40 in air jet when Re is near 100,000. *So et al. [19]* reported self-preservation for x/D larger than about 20 for binary gas jet at Re of 4,300. Although there appear to be some inconsistencies in this criteria, one expects to reach to a similarity profile at the last few axial distances measured here. What emerges as immediately obvious in Fig. 7 is the wide tail in the profiles particularly for the subcritical

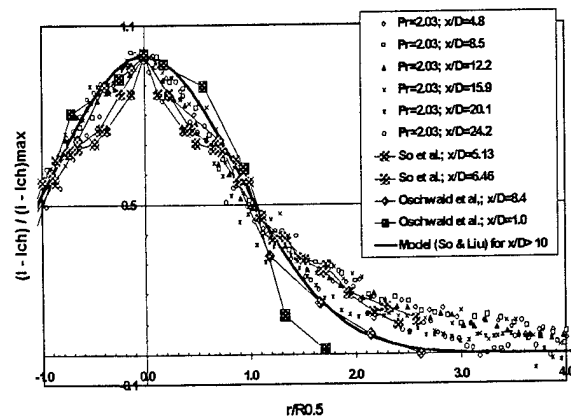


Figure 8. Similar to Fig. 7 but results by other investigators are also shown.

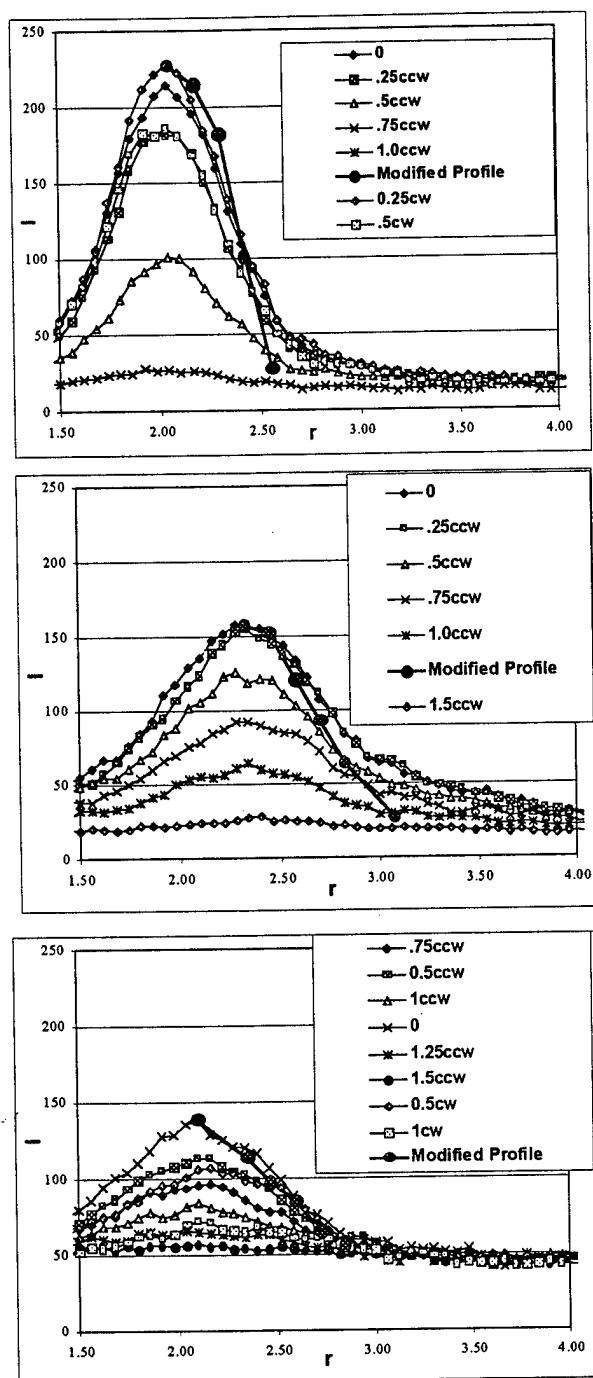


Figure 9. Dark-count-corrected Raman intensity (I) profiles at several different horizontal traverse locations but at a fixed distance from the injector exit ($x/D=12.2$). The Laser sheet is parallel to the axis of the jet and is traversed horizontally towards or away from the camera. The symbol "0" means laser sheet passes through the jet axis; "1ccw" means a 0.5mm shift from the jet axis towards the camera direction; and "1cw" means a 0.5mm shift from the jet axis away from the camera. $Pr=0.43$ (top), 0.83 (middle), and 2.03 (bottom).

case. Also, the profiles appear to be flatter near the center for the subcritical case exhibiting a tendency for a

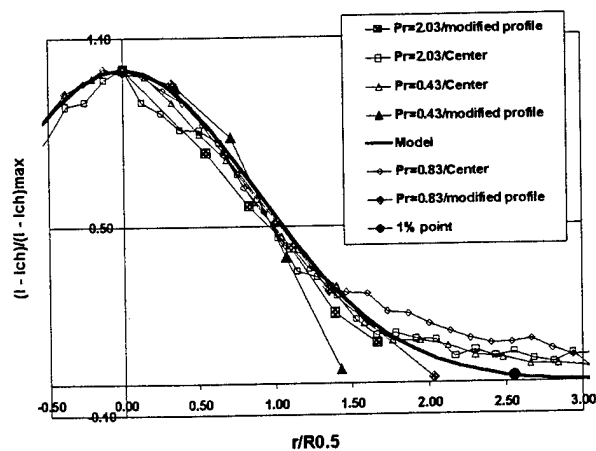


Figure 10. Normalized plot of the Modified and center (i.e. "0") profiles shown in Fig. 8. $x/D=12.2$

near top-hat shape in this region. In Fig. 8 results by *So et al. [19]* (gaseous jets) and *Oswald et al. [13]* (supercritical cryogenic jets) are also shown. They clearly point to difficulties in obtaining high spatial resolution and fidelity information at these distances from the injector exit plane. Note that the outer part of the *So et al.* profiles agree with our data whereas those by *Oswald et al.* follows the model at x/D of 8.4. Although only two profiles are shown, data by *Oswald et al. [13]* appears to be more intuitive as it suggests a gradual change of the shape with distance towards the far field model.

To investigate the causes for the aforementioned profile broadening, the vertical laser sheet was traversed horizontally towards and away from the camera and results were analyzed at several selected axial positions. Figure 9 shows results from such an experiment. A modified profile is then constructed using the maximum values of the Raman intensity profiles at each horizontally-traverse position as indicated in Fig. 9. It is seen that this modified profile is narrower than the profile taken when the laser sheet slices the jet containing the centerline (i.e. the "0" case in Fig. 9). This effect is particularly strong at the subcritical conditions and almost negligible when supercritical. This suggests that reflection from the jet boundary may induce additional Raman effect in this zone causing broadening of the intensity surplus profiles indicated earlier. Considering the injector hole diameter used in this study, such a broadening is to be expected.

Figure 10 shows similarity-type plots for the modified and their corresponding center (identified as "0" in Fig. 9) profiles. The $R_{0.5}$ point is determined for each profile independently. The single solid circle shows the end of the 1% point to be at about 2.5 times the full width at the half maximum (FWHM) value (i.e. $2 \cdot R_{0.5}$). These modified plots suggest lack of type of similarity seen in gaseous turbulent jets at the lowest subcritical condition (i.e. $Pr=0.43$). In contrast, tendency towards such a similarity is observed at Pr of 0.83 and 2.03. Admittedly, the agreement is not perfect. Comparing the modified

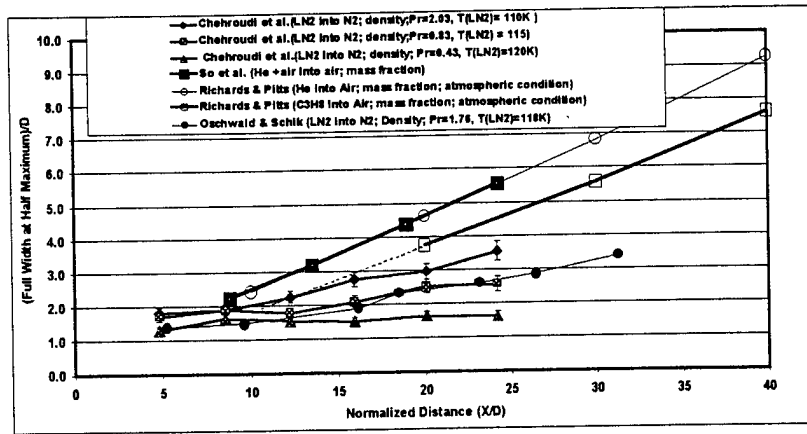


Figure 11. Normalized FWHM of the density surplus radial profiles as a function of the normalized Distance from the injector.

instead the FWHM appears to be a safer parameter to determine. Also, there is doubt if density values can be measured to within 1% accuracy. Nevertheless, *Brown and Roshko* [20] reported that their 1% thickness definition corresponded fairly well with the extent of the mixing visible on the shadowgraph images. However, the spread angle based on the density profile was always larger than that on the velocity profile.

The FWHM at each axial position was determined and results along with data by other investigators are shown in Fig.

	Fluid Inj/Cham	T _{inj} K	P _{ch} MPa	T _{ch} K	Reduced Pressure Pr	Inj/Chamber Density Ratio	D mm	L/D	x/D	Re
Oschwald et al.	N ₂ /N ₂	118	4	298	1.17	3.34	1.9	11.5	8.42	115000 in Figs. 7, 8
Oschwald et al.	N ₂ /N ₂	140	4	298	1.17	12.5	1.9	11.5	1.05	126000 in Figs. 8
Chehroudi et al.	N ₂ /N ₂	95	6.9	295	2	7.1	0.505	100	4.8 to 24.4	35000 in Figs. 8, 10, 11
Chehroudi et al.	N ₂ /N ₂	110	1.5	295	0.4	40.6	0.505	100	4.8 to 24.5	12000 in Figs. 10, 11
So et al.	(He+Air)/Air	275	0.1	275	0.08	0.64	9.5		5.1	5000 in Figs. 8, 11
So et al.	(He+Air)/Air	275	0.1	275	0.08	0.64	9.5		8.4	5000 in Figs. 8, 11
Richards & Pitts	He into Air	275	0.1	275	0.44	0.138	6.35	50	20-80	4000 in Fig. 11
Richards & Pitts	C ₃ H ₈ into Air	275	0.1	275	0.02	1.56	6.35	50	40-120	25000 in Fig. 11

Table 1. Some information extracted from works by other investigators reported here.

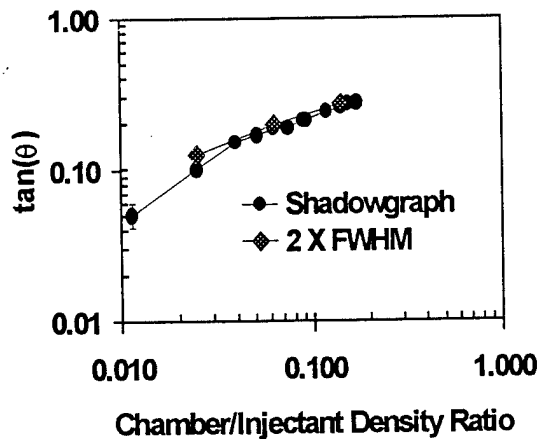


Figure 12. Comparison of the spreading angle measured using shadowgraph and Raman techniques using twice the FWHM values.

profiles with the ones taken at the center, one can deduce the FWHM from these center profiles with not more than a 5% inaccuracy despite the existence of the broadening effect. When available, the best value for the FWHM were considered. The observed broadening in this work prevents us from using the 1% free stream density definition used by *Brown and Roshko* [20] and

11. More information on the conditions under which experiments were performed is given in Table 1. Note that except for *Chehroudi et al.* [8, 9] and *Oschwald et al.* [13] all others are for injection of gaseous fluids into an ambient gas at subcritical pressure (based on the injectant critical pressure). The results of present work in Fig. 11 show an increasingly larger spreading rate as chamber pressure is raised. The data at the supercritical condition ($P_r = 2.03$) approaches that by *Richards and Pitts* [21] acquired at density ratio of larger than 1 even though it is substantially smaller than ours. Unfortunately, for our jets, data at larger distances are not available at present time to develop a more comprehensive comparison between the cases. *Richards and Pitts* [21] conclude that if care is exercised to ensure that flow is free of buoyancy and coflow effects, the spreading rate in variable-density jets is independent of the initial density ratio, velocity profile, turbulence level, and conforms with the results of constant-density by others and, in addition, they propose a slope in the range between 0.212 to 0.220 for this linear jet growth rate equation, see Fig. 11. Our data at $Pr=2.03$ gives a least-square fit to a line with a slope of 0.102, almost half of that by *Richards and Pitts* [13]. It is therefore possible that at some high enough injectant-to-chamber density ratio the spread rate universality indicated by them breaks down and one observes a retarded growth rate for variable-density turbulent jets.

The measured spreading rate using Raman is compared with the spreading rate we reported in the past from the shadowgraph visualizations. The results are plotted in Fig. 12. It can be seen that the spreading rate at twice the FWHM values agrees well with the shadowgraph measurements. At subcritical, a factor less than 2 would give a better agreement as implied from Figs. 10 and 12. Thus the correspondence of the two different techniques for measuring the width of the jet has been established.

Conclusions and Summary

Two-dimensional Raman signal scattered from a cryogenic LN2 jet was acquired at several distances from the injector both at sub- and supercritical conditions. Reflection of the laser off of the jet boundary produced additional Raman effect in this zone causing profile broadening. This effect was demonstrated through systematic horizontal traverses of the laser sheet towards and away from the camera. Within experimental accuracy, the modified intensity surplus plots indicated a similarity behavior of the type observed for classical constant and variable-density gaseous/liquid jets only at near- and super-critical conditions. Because of this broadening effect and as far as a good measure of the jet thickness and growth rate are concerned, the FWHM of the profile is a better estimator to use than the 1% (above the) far field value. The growth rate of the LN2 jet, using slope of the linear FWHM/D versus x/D plot, increases monotonically as chamber pressure reaches critical and supercritical values. A tendency exists for the above linear FWHM plot at supercritical condition to approach those reported for gaseous jets affirming our gas-like appearance reported in the past. It is also shown that a plot of twice the FWHM versus density ratio agrees with the jet thickness measured through our shadowgraphy studies. This establishes an equivalency between these two different jet thickness determination methods.

Acknowledgement

Mr. Mike Griggs and Mr. Earl Thomas are thanked for their valuable support. We also appreciate Mr. Mike McKee's contribution in part of the data acquisition. This work is sponsored by the Air Force Office of Scientific Research under Mr. Mitant Birkan, program manager.

References

1. Mayer, et al. "Injection and mixing processes in high pressure LOX/GH2 rocket combustors," AIAA Paper no. 96-2620, Lake Buena Vista, Florida, 1996.
2. Mayer, et al. "Propellant atomization in LOX/GH2 rocket combustors," AIAA Paper no. 98-3685, 1998.
3. Chen, L.-D. and Sui, P.-C. "Atomization during the injection of supercritical fluid into high pressure environment," in *Mechanics and Combustion of Droplets in Sprays* by Chiu and Chigier.
4. Woodward, R. D. and Talley, D. G. "Raman imaging of transcritical cryogenic propellants," AIAA Paper 96-0468, Reno, Nevada, January 1996.
5. Harstad, K and Bellan, J. "Isolated fluid oxygen drop behavior in fluid hydrogen at rocket chamber pressures," *International Journal of Heat and Mass Transfer* 41, pp. 3537-3550, 1998.
6. Delplanque J. P. and Sirignano W. A. "Atomization and Sprays," 4:325-349, 1994.
7. Oefelein, J. C. and Yang V. "Modeling High-pressure Mixing and combustion Processes in Liquid Rocket Engines," *J. Propulsion & power*, Vol. 14, no. 5, September-October, 1998.
8. Chehroudi, B., Talley, D.G., and Coy, E.B., "Initial Growth Rate and Visual Characteristics of a Round Jet into a Sub- to Supercritical Environment of Relevance to Rocket, Gas Turbine, and Diesel Engines," AIAA paper 99-0206, Reno, Nevada, 1999.
9. Chehroudi, B., Talley, D., and Coy, E. "Fractal geometry and growth rate of cryogenic jets near critical point," AIAA Paper 99-2489, 35th AIAA/ASME/SAE/ASEE Joint Propulsion Conference, Los Angeles, CA, June 20-24, 1999.
10. Anderson, T.J., Woodward, R.D., and Winter, M. "Oxygen Concentration Measurements in a High Pressure Environment Using Raman Imaging," AIAA Paper 95-0140, 33rd Aerospace Sciences Meeting and Exhibit, January 9-12, Reno, NV, 1995.
11. Decker, M C, Schik, A, Meier, U E, Stricker R W. "Quantitative Raman Imaging Investigations of Mixing Phenomena in High Pressure Cryogenic Jets," *Appl Opt* 37:5620-5627, 1998.
12. Oschwald, M. and Schik, A. "Supercritical Nitrogen Free Jet Investigated by Spontaneous Raman Scattering," *Experiments in Fluids*, 27, 497-506, 1999.
13. Oschwald, M, Schik, A, Klar, M, Mayer, W, "Investigation of Coaxial LN2/GH2-Injection at Supercritical Pressure by Spontaneous Raman Scattering," 35th AIAA/ASME/SAE/ASEE Joint Propulsion Conference and Exhibit, Los Angeles, CA, 20-24 June, 1999.
14. Schlichting, H. *Boundary Layer Theory*, MacGraw-Hill Book Company, seventh edition, 1979.
15. Brown G., "The entrainment and large structure in turbulent mixing layers," 5th Australasian Conf. on Hydraulics and Fluid Mech., 1974, pp. 352-359.
16. Papamoschou, D. and Roshko, A. "The compressible turbulent shear layer: an experimental study," *J. Fluid Mech.*, vol. 197, 1988, pp. 453-477.
17. Dimotakis, P. E. "Two-dimensional shear-layer entrainment," *AIAA Journal*, 21, No. 11, 1986, pp. 1791-1796.
18. Wygnanski, I and Fiedler, H. E. "The two-dimensional Mixing region," *J. Fluid Mech.*, 41, 327, 1970.
19. So, R M C, Zhu, J Y, Otugen, M V, and Hwang, B C, "Some Measurements in a Binary Gas Jet," *Experiments in Fluids*, 9, 273-284, 1990.
20. Brown, G. and Roshko, A. "On density effects and large structure in turbulent mixing layers," *J. Fluid Mech.*, vol. 64, 1974, part 4, pp. 775-816.
21. Richards, C. D. and Pitts, W. M. "Global density effects on the self-preservation behavior of turbulent free jets," *J. Fluid Mech.*, Vol. 254, 1993, pp. 417-435.